Protein Science (1996), *5*:1342–1354. Cambridge University Press. Printed in the USA.
Copyright © 1996 The Protein Society

Cytochrome c_3 from *Desulfovibrio gigas*: Crystal structure at 1.8 Å resolution and evidence for a specific calcium-binding site

PEDRO M. MATIAS,[1] JOSÉ MORAIS,[1] RICARDO COELHO,[1]
MARIA ARMÉNIA CARRONDO,[1,2] KEITH WILSON,[3]
ZBIGNIEW DAUTER,[3] AND LARRY SIEKER[1,4]

[1] Instituto de Tecnologia Química e Biológica, Universidade Nova de Lisboa, 2780 OEIRAS, Portugal
[2] Instituto Superior Técnico, Universidade Técnica de Lisboa, 1000 LISBOA, Portugal
[3] European Molecular Biology Laboratory, c/o DESY, Notkestrasse 85, D-22603 Hamburg, Germany
[4] Department of Biological Structure, University of Washington, Seattle, Washington 98195

(RECEIVED January 5, 1996; ACCEPTED April 11, 1996)

Abstract

Crystals of the tetraheme cytochrome c_3 from sulfate-reducing bacteria *Desulfovibrio gigas* (Dg) (MW 13 kDa, 111 residues, four heme groups) were obtained and X-ray diffraction data collected to 1.8 Å resolution. The structure was solved by the method of molecular replacement and the resulting model refined to a conventional *R*-factor of 14.9%. The three-dimensional structure shows many similarities to other known crystal structures of tetraheme c_3 cytochromes, but it also shows some remarkable differences. In particular, the location of the aromatic residues around the heme groups, which may play a fundamental role in the electron transfer processes of the molecule, are well conserved in the cases of hemes I, III, and IV. However, heme II has an aromatic environment that is completely different to that found in other related cytochromes c_3. Another unusual feature is the presence of a Ca^{2+} ion coordinated by oxygen atoms supplied by the protein within a loop near the N-terminus. It is speculated that this loop may be stabilized by the presence of this Ca^{2+} ion, may contribute to heme-redox perturbation, and might even be involved in the specificity of recognition with its redox partner.

Keywords: calcium binding; crystallography; cytochrome c_3; structure

Cytochrome c_3 is a tetraheme cytochrome (MW ca. 13 kDa) found in sulfate-reducing bacteria. The four heme groups are covalently bound to a single polypeptide chain of 111 amino acid groups via thioether bridges to cysteine residues. All heme axial ligands are histidines rather than the histidine and methionine arrangement found in the monoheme *c*-type cytochromes. Cytochrome c_3 has been the subject of a variety of studies because of the unusual heme content of this molecule, the low midpoint redox potential of the iron atoms in these multiheme molecules, which can range from −120 to −400 mV, and because of the intramolecular electron exchange between the hemes. Each heme of cytochrome c_3 has a different midpoint redox potential and they show variable redox cooperativity between them (Santos et al., 1984; Piçarra-Pereira et al., 1993).

Crystal structures of several cytochrome c_3 molecules have been determined. These include the cytochromes from *Desulfovibrio vulgaris* strain Miyazaki F (DvMF) at 1.8 Å (Higuchi et al., 1984), *Desulfomicrobium baculatus* strain Norway 4 (DmbN) at 1.7 Å (Czjzek et al., 1994), *D. vulgaris* strain Hildenborough (DvH) for orthorhombic crystal forms at 2.0 Å (Morimoto et al., 1991; Higuchi et al., 1994) and hexagonal at 1.9 Å (Matias et al., 1993), an incomplete model for *D. gigas* (Dg) at 2.4 Å (Kissinger, 1989; Matias et al., 1994), *D. desulfuricans* ATCC 27774 (Dd) at 1.8 Å (Morais et al., 1995), and finally *Dm. baculatus* ATCC 9974 (Dmb) at 1.8 Å (Coelho et al., 1995). All show the same general fold of the polypeptide chain, except where deletions and insertions occur.

A comparison of the amino acid sequences of the polypeptide chain of these small proteins shows a surprising variation in sequence homology in spite of the invariant set of residues involved in coordinating the hemes. Figure 1 shows the sequence alignment for four of the cytochrome c_3 molecules for which three-dimensional structures have been determined. It can be seen that, among these molecules, except for the cysteine and histidine residues, there is only slight homology for the rest of the polypeptide chain. In some cases, there are significant insertions and deletions in selected locations. This diversity pre-

Reprint requests to: Maria Arménia Carrondo, ITQB-UNL, Apartado 127, 2780 OEIRAS, Portugal; e-mail: carrondo@itqb.unl.pt.

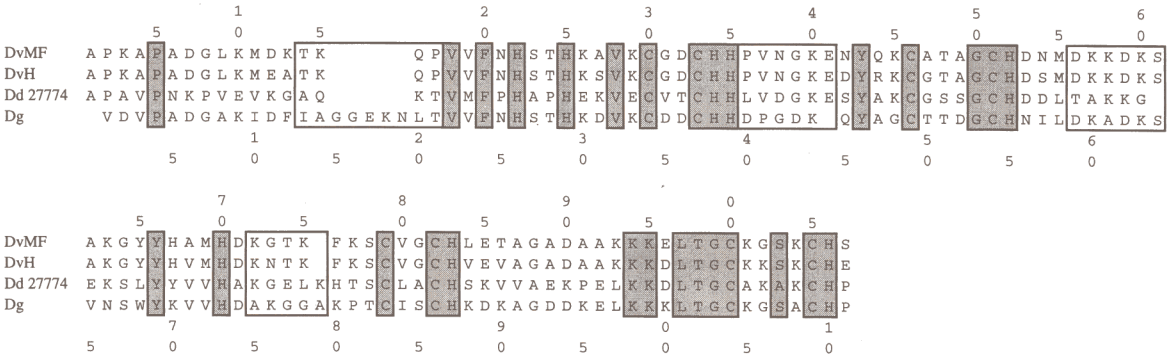

Fig. 1. Sequence alignment of four cytochrome c_3 molecules. The top sequence numbering scheme refers to DvMF and DvH (107 aa) while the bottom one refers to Dg (111 aa). The shaded boxes indicate the aminoacid residues common to all four sequences. The open boxes represent loop regions where there can be residue insertions or deletions between c_3 molecules from different organisms.

sumably causes different environmental conditions around each heme, resulting in a different redox potential, varying pH dependencies, and rates of intramolecular electron transfer exchange. The availability of three-dimensional structures of several tetraheme cytochromes allows a more comprehensive investigation into the characteristics of these molecules.

The amino acid sequence of cytochrome c_3 from *D. gigas* (c_3Dg) contains some significant differences that should contribute to our understanding of the functional aspects of these tetraheme cytochromes. This particular molecule has a pI of 5.2(2), which is much lower than found for the other tetraheme cytochromes (LeGall et al., 1963).

In this report, a well-refined structural model at 1.8 Å for c_3Dg is presented.

Results

A stereo view of the c_3Dg molecule is represented in Figure 2, showing the C^{α} skeleton, the bound Ca^{2+} ion, and the hemes, together with the side chains of the cysteine and histidine residues attached to them. Figure 3 (see Kinemage 1) shows a stereo view of the Ca^{2+} coordination within the loop comprising residues Asp 11–Leu 20, where it is octahedrally coordinated to oxygens from two carbonyl groups, Ile 13 and Leu 20, $O^{\delta 1}$ of carboxylate from Asp 11 and $O^{\delta 1}$ from Asn 19, and one oxygen, O^{1A} and O^{2D} from each propionate of heme IV. The hemes are bound to the polypeptide chain through covalent bonds between heme atoms C^{AB} and C^{AC}, and S^{γ} atoms of the cysteine residues.

Figure 4 shows a Ramachandran plot (Ramachandran & Sasisekharan, 1968) for the refined model of the polypeptide chain, and only Cys 54 lies clearly outside the normally allowed regions for non-glycine residues. The program package PROCHECK (Laskowski et al., 1993) was used to assess the stereochemical quality of the model, and all parameters are well within their confidence intervals. In the course of refinement, there were some atoms for which no significant electron density could be observed in either the $2|F_o| - |F_c|$ or the $|F_o| - |F_c|$ Fourier maps, and were therefore assigned zero occupancy. A list of these is given in Table 1. Most of them correspond to side-chain atoms of lysine residues, and all the residues for which no density beyond C^{α} could be observed were modeled as alanine residues in the final refinement.

The RMS error in the refined atomic coordinates has been estimated as 0.06 Å by means of a SIGMAA plot (Read, 1986). Figure 5A shows the average error in the refined atomic coordinates per residue for main-chain and side-chain atoms, obtained from the individual atomic positional parameter estimated standard deviations (ESDs). The overall average coordinate error estimated in this manner is also 0.06 Å. This plot is useful because it shows, unlike the SIGMAA plot, the variation

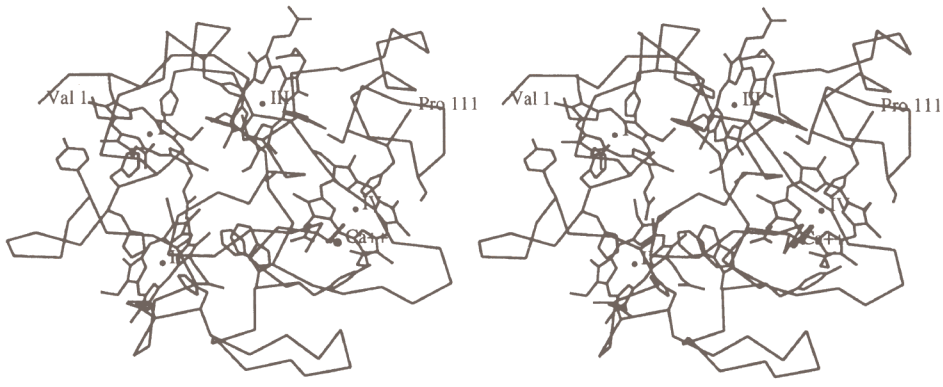

Fig. 2. Stereo view of c_3Dg molecule showing the C^{α} skeleton, the Ca^{2+} ion, the hemes, and the side chains of the histidine and cysteine residues attached to them, and also the side chains of the aromatic residues. Drawing made with TURBO (Roussel et al., 1990).

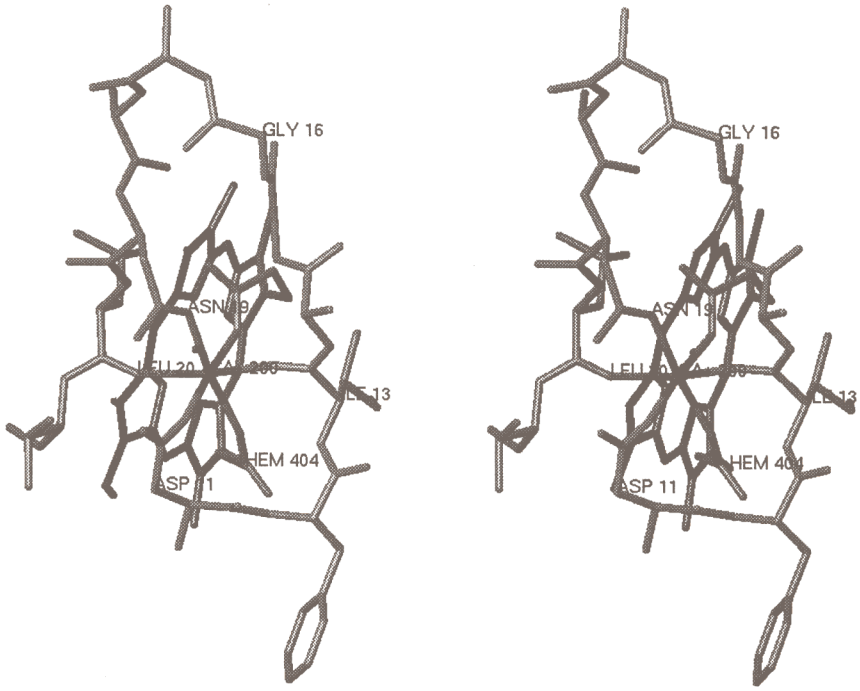

Fig. 3. Stereo view of the Ca^{2+} binding loop in c_3Dg. Drawing made with TURBO (Roussel et al., 1990).

in coordinate error as a function of residue number. Figure 5B is a plot of the average temperature factors for main-chain and side-chain atoms as a function of residue number. The corresponding average values for the heme groups are given in Table 2. The variation in both average main-chain and side-chain *B*-factors along the protein chain show a similar pattern to that of the average main-chain and side-chain coordinate errors in Figure 5A. This can be appreciated in Figure 6, where the average *B*-factor is plotted against coordinate error, for both main-chain and side-chain atoms, and a positive correlation can be seen clearly. The *B*-values of the solvent molecules ranged between 12.2 and 46.7, with an average value of 28.3.

Discussion

The structure of the c_3Dg molecule was analyzed and compared mainly with those of c_3DvH and c_3DvMF. Some additional

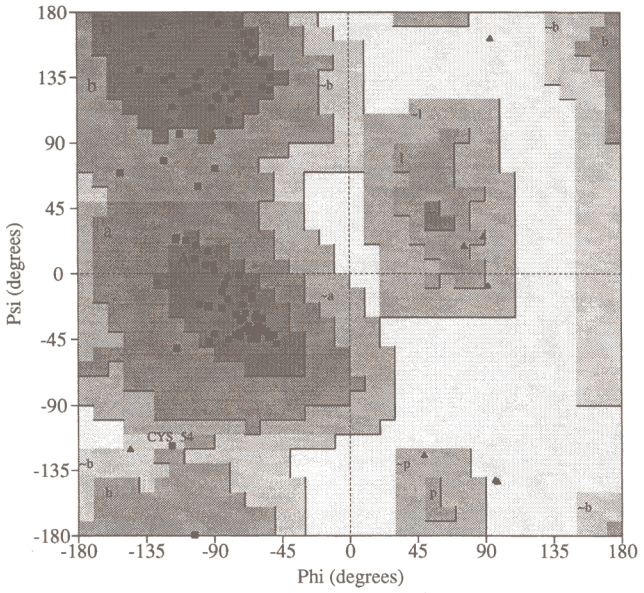

Fig. 4. ϕ,ψ plot (Ramachandran & Sasisekharan, 1968) for c_3Dg. Glycine residues are represented by triangles, other residues by squares. Drawing made with program PROCHECK (Laskowski et al., 1993).

Table 1. *Dummy atoms in the refined structure of c_3Dg cytochrome*

Residue no.	Missing atoms
Asp 2[a]	C^{γ}-$O^{\delta 2}$
Lys 9[a]	C^{γ}-N^{ζ}
Glu 17[a]	C^{γ}-$O^{\epsilon 2}$
Lys 18[a]	C^{γ}-N^{ζ}
Lys 30	C^{δ}-N^{ζ}
Lys 33	N^{ζ}
Asp 40[a]	C^{γ}-$O^{\delta 2}$
Asp 43	$O^{\delta 1}$, $O^{\delta 2}$
Lys 44	C^{ϵ}, N^{ζ}
Lys 63	C^{ϵ}, N^{ζ}
Lys 88[a]	C^{γ}-N^{ζ}
Lys 90[a]	C^{γ}-N^{ζ}
Asp 93	$O^{\delta 1}$
Lys 95[a]	C^{γ}-N^{ζ}
Glu 96	C^{γ}-$O^{\epsilon 2}$
Lys 98	C^{ϵ}, N^{ζ}
Lys 99	C^{δ}-N^{ζ}
Lys 105	C^{ϵ}, N^{ζ}

[a] Due to the lack of density for side-chain atoms, these residues were modeled as alanines.

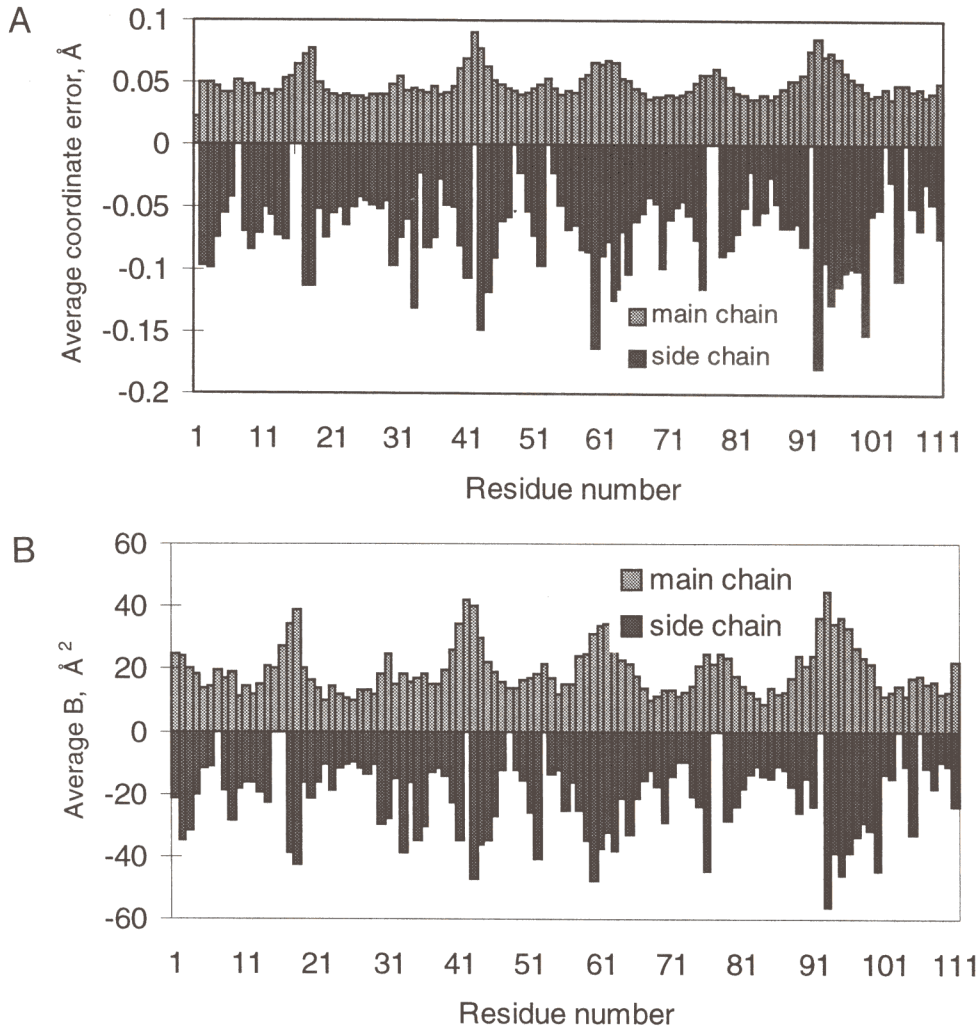

Fig. 5. A: Plot of the main-chain (above *x*-axis) and side-chain (below *x*-axis) average coordinate errors estimated from the atomic parameter ESDs obtained in the final full-matrix blocked refinement. **B:** Plot of the main-chain (above *x*-axis) and side-chain (below *x*-axis) average temperature factors per residue in c_3Dg.

comparisons with c_3DmbN and c_3Dd are included in this section where deemed appropriate or interesting. In this study, we follow the same heme numbering scheme adopted in our earlier report on the structure of the hexagonal crystal form of c_3DvH (Matias et al., 1993), which differs from that adopted by Higuchi et al. (1984).

Table 2. *Average B values and RMS differences for the heme groups*

Heme	c_3Dg Average *B* (Å^2)	RMS difference to c_3DvH A (Å)		
		Overall	Heme ring[a]	Propionate[b]
I	16.9	1.12	0.37	2.23
II	17.0	0.86	0.52	1.51
III	14.6	0.61	0.34	1.11
IV	10.9	1.36	0.48	2.69

[a] The heme ring includes the four pyrrole ring atoms and all atoms attached to them directly.
[b] The propionate side-chain atoms except C^{AA} and C^{AD}.

Molecular structure

The tertiary structure of the c_3Dg molecule is similar to that of c_3DvMF and c_3DvH. Figure 7 shows a superposition of the C^{α} skeleton of c_3Dg, c_3DvH molecule A, and c_3DvMF, and the three loop regions where the structural differences are most pronounced are indicated. The secondary structure elements are similar to those in DvH and DvMF, with short α-helices between S67 and D74, T82 and G92, and D94 and G103, and two very short 3_{10} helices between H26 and K30 and K33 and C37. However, only one very short two-stranded antiparallel β-sheet, A8–I10 to V22–F24 is found in c_3Dg, because the second sheet in c_3DvH (H35–V37 to K40–N42) and c_3DvMF (H35–V37 to K40–D42) occurs in a region where there has been a deletion in c_3Dg; furthermore, one of the residues that might be involved in the first strand (V37 in DvH and DvMF) has been changed into a proline (P41 in Dg), effectively blocking the possibility of the N atom donating a hydrogen bond. In addition, this region

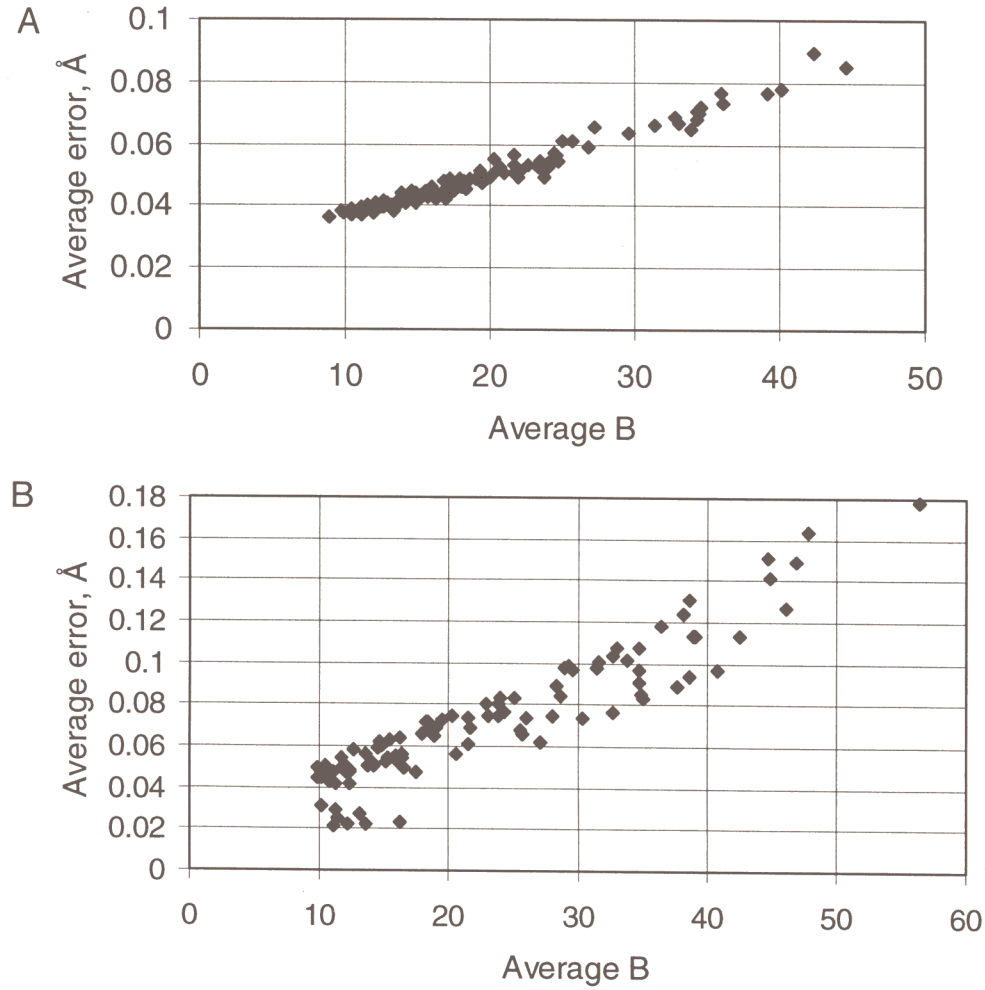

Fig. 6. A: Plot of the average temperature factors versus average coordinate errors per residue for main-chain atoms in c_3Dg. **B:** Plot of the average temperature factors versus average coordinate errors per residue for side-chain atoms in c_3Dg.

(H39–Q45 in Dg) adopts a different conformation from that found in c_3DvH and c_3DvMF. The unusual ϕ,ψ conformation of Cys 54 (shown in Fig. 4) is also found in both c_3DvMF and c_3DvH structures, where it corresponds to Cys 51.

A plot of the RMS difference in atomic positions of main-chain atoms for the common backbone regions of c_3Dg, c_3DvMF, and c_3DvH (molecule A) after superimposing the three structures (not shown) confirms that the largest deviations

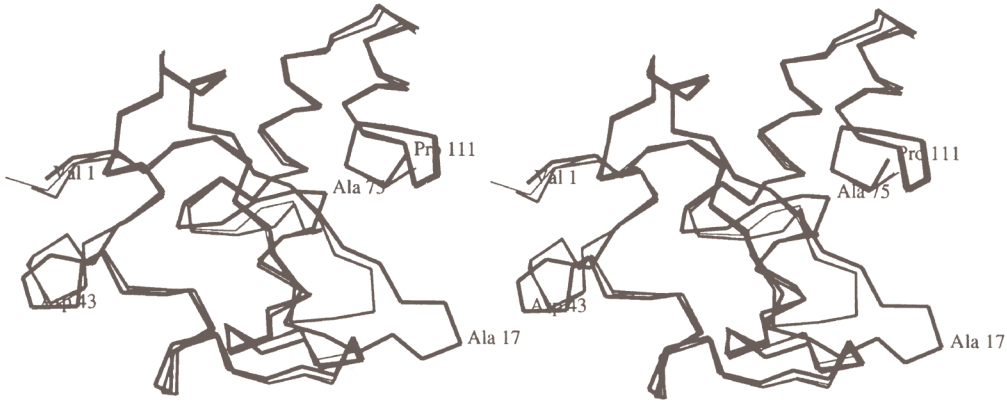

Fig. 7. Stereo view of the superimposed C^{α} skeletons of c_3Dg (thick line), c_3DvH molecule A (medium thickness line), and c_3DvMF (thinner lines). The residues Ala 17, Asp 43, and Ala 75 mark the regions in c_3Dg where the differences with the other two molecules are largest. Drawing made with TURBO (Roussel et al., 1990).

occur in the regions where the polypeptide chain of c_3Dg has insertions or deletions with respect to that of c_3DvH (see also Fig. 1). The corresponding RMS difference in atomic positions for the heme groups are presented in Table 2, and in comparison with similar values between c_3DvH and c_3DvMF (Table 9 in Matias et al., 1993), the deviations between the heme atomic positions in c_3Dg and c_3DvH are larger. However, as shown in Table 2, the main source of these higher deviations lies not in the heme rings per se, but rather in the termini of the propionate groups, which adopt different conformations in c_3Dg, particularly for hemes I and IV. Heme II has the higher average *B*-factor in most of the known structures, c_3DvH, c_3DmbN, c_3Dd, and also in c_3Dg.

Heme environment

All comparisons that follow between c_3Dg and other cytochrome c_3 structural models were carried out using the results from parallel calculations using the same programs and protocols, in order to avoid any bias arising from differences in calculation methods.

Intramolecular heme iron–iron distances, edge to edge distances of the porphin rings, and interplanar angles are listed in Table 3. These values are consistent with the results obtained for c_3DvH and c_3DvMF (Table 10 in Matias et al., 1993). The environment of the iron atoms in c_3Dg is very similar to that found previously in the three molecules c_3DvH A, B, and DvMF (Table 11 in Matias et al., 1993).

The coordination geometry of the iron atoms to the ligated histidines can be characterized by some selected angles listed in Table 4, such as the angle between the $N^{\epsilon 2}$-Fe line and the two heme planes as defined above, and the tilt of the histidines relative to those heme planes. Other relevant angles include the orientation of the histidine normals in relation to the diagonal line N^C-N^A on the heme plane and the angle between the two histidine ring normals on both sides of each heme. These angles have been calculated for the c_3Dg structure and none differ significantly from those obtained previously (Table 12 in Matias et al., 1993).

In a similar fashion to c_3DvMF and c_3DvH, and apart from residue numbering differences due to insertions and deletions in the c_3Dg chain, hemes II and IV are bound to Cys 49 and Cys 54 and to Cys 104 and Cys 109, respectively, with four residues in between, whereas hemes I and III are bound to Cys 34 and Cys 37, and to Cys 83 and Cys 86, respectively, with two residues in between. The torsion angles χ_1, χ_2, and χ_3 listed in Table 5 show that the geometry of the cysteine–heme linkage in c_3Dg is also similar to that in c_3DvMF and c_3DvH (Table 13 in Matias et al., 1993).

There are a few aromatic residues that are conserved among all six cytochromes c_3 of known sequence (see, for example, Table 2 in Matias et al., 1993) that are involved in interactions with both adjacent histidine residues and heme pyrrole rings.

In c_3Dg, Phe 24 is nearly perpendicular to His 26 linked to heme I, and almost parallel to both pyrrole ring D in heme I and His 29 attached to heme III. On the other side of heme I, Tyr 46 is nearly parallel to His 38 and close to orthogonal to pyrrole

Table 3. *Intramolecular iron–iron distances and heme–heme angles*

	Angles (°) and distances (Å)[a]			
Heme[b]	I	II	III	IV
I	–	12.0 (6.4)	11.2 (6.0)	18.0 (10.7)
II	86.7	–	15.5 (8.3)	16.7 (10.8)
III	83.5	59.9	–	12.0 (5.5)
IV	20.9	70.6	81.2	–

[a] Angles are given below the center diagonal; distances are given above it. Distances in parentheses refer to the nearest distance between porphin atoms.
[b] Heme planes are calculated for all atoms in the porphin ring.

Table 4. *Selected angles (°) for the coordination geometry of ligated histidines*[a]

		Heme[b] (pyrrole [c]) plane and		His plane normal and	
Heme		Vector $N^{\epsilon 2}$-Fe	His plane[d]	Vector N^C-N^{Ae}	His plane normal
I	His 26	88.0 (87.4)	88.4 (88.9)	33.5	4.0
	His 38	87.4 (89.6)	88.1 (85.5)	35.7	
II	His 39	88.3 (89.3)	80.6 (82.9)	−17.6	52.0
	His 55	87.4 (87.8)	87.2 (88.2)	35.9	
III	His 29	86.1 (88.9)	80.4 (79.2)	−67.8	13.6
	His 87	87.9 (87.8)	86.4 (87.5)	−64.4	
IV	His 73	85.3 (86.2)	88.1 (89.0)	36.0	15.0
	His 110	84.3 (85.3)	78.9 (79.9)	26.0	

[a] Atoms in the heme groups are named according to standard nomenclature in the Protein Data Bank (Bernstein et al., 1977).
[b] Least-squares heme plane is defined by the four pyrrole ring atoms and all atoms attached to them directly.
[c] Least-squares plane of the four heme nitrogen atoms.
[d] Least-squares plane of histidine imidazole ring.
[e] His planes with positive sign lie between N^A-Fe-N^D and those with a negative sign between N^A-Fe-N^B.

Table 5. *Geometry of cysteine–heme linkages in c_3Dg*

Heme		χ_1[a] (°)	χ_2[b] (°)	χ_3[c] (°)
I	Cys 34	−42.5	−68.7	−50.9
	Cys 37	−53.7	179.9	−51.1
II	Cys 49	−45.4	−67.9	−57.6
	Cys 54	−56.7	−79.7	−46.1
III	Cys 83	−43.6	−81.5	−36.9
	Cys 86	169.6	179.1	64.5
IV	Cys 104	−51.2	−55.2	−40.8
	Cys 109	−58.0	−165.3	−31.0

[a] Angle N-C^{α}-C^{β}-S^{γ}.
[b] Angle C^{α}-C^{β}-S^{γ}-C^{AB}-(C^{AC}).
[c] Angle C^{α}-S^{γ}-C^{AB}-(C^{AC})-C^{3B}(C^{3C}).

ring B. Similar relative orientations are found with the equivalent residues in c_3DvH and c_3DvMF.

Hemes III and IV have likewise similar environments in c_3Dg, c_3DvH, and c_3DvMF, with a phenylalanine residue parallel to one of the histidines and perpendicular to the pyrrole ring B of heme III (Phe 20 and His 25 in c_3DvH and c_3DvMF, Phe 24 and His 29 in c_3Dg), and a tyrosine residue parallel to a histidine and orthogonal to ring A of heme IV (Tyr 66 and His 70 in c_3DvH and c_3DvMF, Tyr 69 and His 73 in c_3Dg).

However, heme II has a completely different aromatic residue environment in c_3Dg. Whereas in c_3DvH and c_3DvMF Phe 76 was approximately parallel to His 35 and orthogonal to pyrrole ring A of heme II, in c_3Dg Phe 76 has been replaced by Lys 80. On the other side of heme II, Trp 68 is orthogonal to both pyrrole ring B and Phe 12, which, in turn, is exposed to solvent. These two aromatic residues are unique to c_3Dg. In the three-dimensional structure of c_3Dg, Trp 68 occupies a position equivalent to Tyr 65 in c_3DvH and c_3DvMF. This Trp 68 is too far from heme II for a direct interaction to be likely. In addition, Trp 68 is nearly orthogonal to the pyrrole ring D of heme IV, and approximately equidistant from both hemes II and IV. Figure 8 shows a stereo view of the superimposed c_3Dg and c_3DvH molecule A, emphasizing the spatial relationship between hemes II and IV, and Trp 68 and Phe 12 in c_3Dg, as opposed to Tyr 65 in molecule A of c_3DvH.

Interesting hydrogen bonds and structural water molecules

The intramolecular hydrogen bonding scheme is generally comparable to that observed in DvH and DvMF, contributing to the fold of the molecules through the formation of three α-helices, two 3_{10} helices, several reverse turns, but only one short β-sheet. Likewise, the hydrogen bonding pattern of the N^{δ}-H groups of the histidine residues coordinated to the heme iron atoms are very similar. Table 6 lists the distances found for such hydrogen bonds and summarizes their comparison with DvH and DvMF. The histidine residues coordinated to hemes I, III, and IV are hydrogen bonded to either conserved water molecules or carbonyl oxygens of conserved residues. In contrast, one of the histidine residues ligated to heme II (His 55) is hydrogen bonded to the carbonyl oxygen of Ala 62, which is not conserved in either DvMF or DvH, whereas the other (His 39) forms an N^{δ}-H$\cdots$O hydrogen bond to a water molecule (Wat 180) instead of the carbonyl atom of Pro 36. These two changes can be attributed to the mutations and deletion in amino acid sequence that occur between His 39 and Tyr 56 in Dg (see Fig. 1) in comparison with DvH and DvMF (between His 35 and Tyr 48). This region comprises a short two-stranded antiparallel β-sheet in DvH and DvMF. However, in Dg, not only is this β-sheet missing, as noted above, but, perhaps more importantly, this region now forms an extended loop that adopts a conformation significantly shifted with respect to that found in DvH and DvMF. As a consequence, and although the relative solvent exposure is lower for Dg His 39 than for DvH/DvMF His 35, the N^{δ}-H group of Dg His 39 is now oriented *toward* the solvent rather than *toward* the protein chain. Figure 9 shows a stereo view of the superimposed c_3Dg and c_3DvH A molecules where the different loop conformations and hydrogen bonding schemes can be appreciated.

Three additional structural features unique to c_3Dg in comparison with the other cytochromes c_3 with known three-dimensional structure are the aromatic residues Phe 12 and Trp 68, and the presence of a bound Ca^{2+} ion. There is an indirect but possibly significant structural connection related to these three features. Indeed, as shown in Figure 10, one of the propionate groups of heme IV coordinates the Ca^{2+} ion through O^{2D} and forms a bifurcated hydrogen bond through O^{1D} to both Trp 68 $N^{\epsilon 1}$ (3.02 Å) and Phe 12 N (2.76 Å), and the angle between the two hydrogen bonds is 120.7°. Atom O^{2D} also forms a hydrogen bond to Ile 13 N (2.95 Å), the angle $Ca^{2+}\cdots O^{2D}\cdots$N being 101°. An interaction between Phe 12, Trp 68, and the Ca^{2+} ion, mediated by a carboxylate group from heme IV, is therefore possible.

A more extensive comparison of the structural waters in the five crystal structures can now be conducted between the cytochromes c_3 from Dg, DvH, DvMF, DmbN, and Dd (see Table 6 above and Table 7 in Morais et al., 1995). The waters that are located on both sides of heme I are conserved in all these struc-

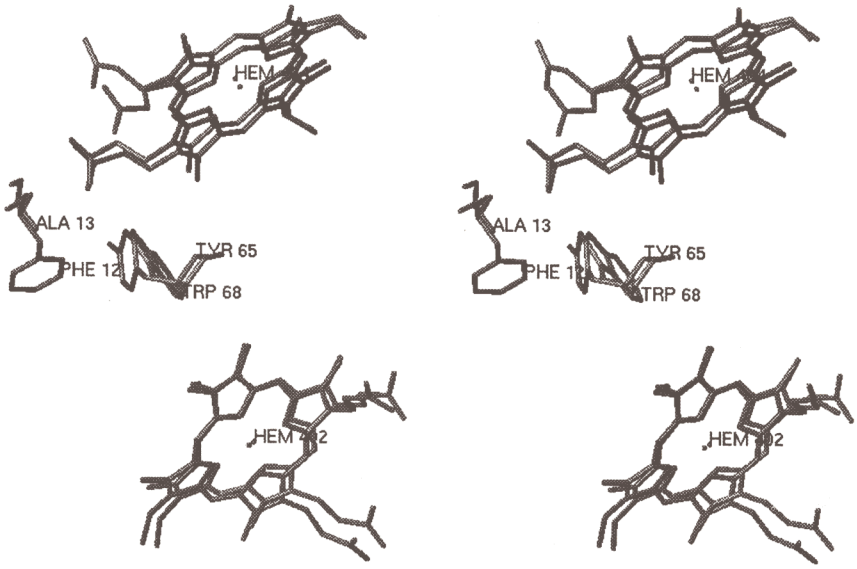

Fig. 8. Stereo view of the superimposed c_3Dg and c_3DvH molecule A, showing the spatial relationship between hemes II and IV, Trp 68, and Phe 12 in Dg; and hemes II and IV, Tyr 65, and Ala 13 in DvH. Phe 12 and Trp 68 are residues unique to c_3Dg and provide a completely different environment for one side of heme II. Drawing made with TURBO (Roussel et al., 1990).

Table 6. *Hydrogen bonds involving ligated histidines in c_3Dg*

Heme	Distances for $N^{\delta 1}$ atoms (Å)		Comparison with c_3DvH and c_3DvMF
I	His 26	O (Wat 128)	2.82 conserved with conserved water molecule
	His 38	O (Wat 121)	2.84 conserved with conserved water molecule
II	His 39	O (Wat 180)	3.20 changed due to mutation/deletion (see text)
	His 55	O (Val 65)	2.78 conserved in spite of mutated residue (Ala 62)
III	His 29	O (Asn 25)	2.87 conserved with conserved residue (Asn 21)
	His 87	O (Leu 101)	2.76 conserved with conserved residue (Leu 97)
IV	His 73	O (Tyr 69)	2.90 conserved with conserved residue (Tyr 66)
	His 110	O (Wat 140)	2.82 conserved with conserved water molecule

tures, making H-bonds to carbonyl oxygen atoms. Similarly, on the side of heme IV where the C-terminal part of the polypeptide chain is located, one water molecule that is H-bonded to neighboring oxygens is also conserved in four of the crystal structures. In c_3DmbN (Czjzek et al., 1994), however, there is an additional water molecule on the opposite side of heme IV involved in a similar H-bond network. This water molecule has a low *B*-factor (W266, 4.6 Å^2), comparable to the *B*-values of the protein in that region and, in particular, to those of the atoms to which it is hydrogen bonded (His 89 Nδ 6.0 Å^2, Glu 85 Oε2 13.2 Å^2). Therefore, those authors claim that this particular situation is responsible for the tilt of that histidine, His 89, relative to His 115 on the other side of heme IV, resulting in an angle of 77° between the two histidine planes. This is very different from what is observed with this heme in all four other cytochrome structures.

Another unique but not comparable situation is described for the orthorhombic form of c_3DvH (Higuchi et al., 1994). Here a water molecule is hydrogen bonded to His 25, which coordinates to heme III. In this case, the geometry of this position does not correspond to any usual H-bonding scheme and, furthermore, the *B*-factor of that atom is 65 Å^2, significantly higher than the range of 8–10 Å^2 observed for its neighboring atoms, making the significance claimed for this water molecule much less reliable.

Solvent accessibility

The relative solvent accessibility was calculated with X-PLOR using the Lee and Richards (1971) algorithm with an H_2O probe radius of 1.6 Å. The calculation was performed in two steps: first, the solvent-accessible surface was calculated for each residue in the structure (abstracting all non-protein atoms), and next the same calculation was done for the same residue isolated from the rest of the structure. The relative solvent accessibility for each residue was then given by the ratio of the two numbers. Figure 11 shows the variation in percent relative solvent accessibility along the polypeptide chain in c_3Dg, whereas Figure 12 contains similar information for the heme groups of c_3Dg, c_3DvMF, c_3DvH (molecules A and B), and c_3Dd. The values in Figure 12 show that the overall heme solvent exposure is highest in c_3Dg, with heme II having a consistently higher value (with the exception of c_3Dd), and heme I having a consistently lower value (with the exception of c_3DvMF). Of all cytochrome c_3 molecules analyzed, heme IV has the highest solvent exposure in c_3Dg, which may be connected with the coordination of

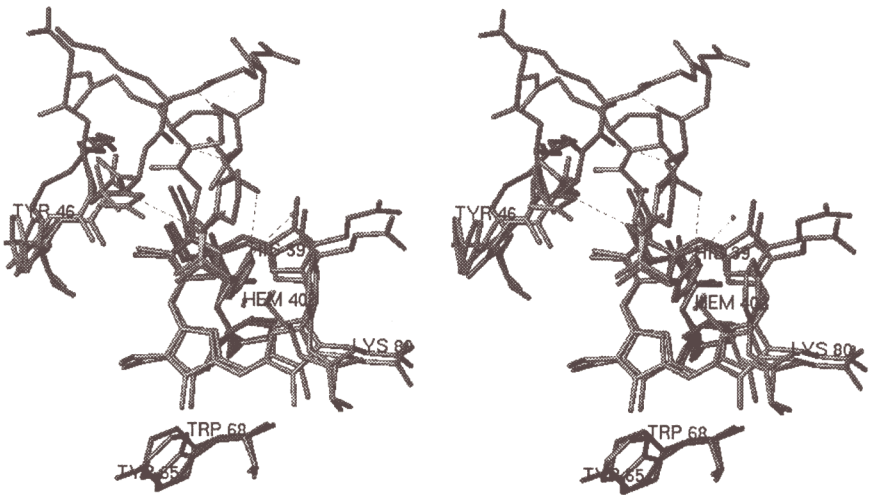

Fig. 9. Stereo view of the superimposed heme II environments in c_3Dg and c_3DvH molecule A, showing the different loop conformations and histidine hydrogen bonding schemes. Atom labels refer to Dg unless explicitly noted otherwise. Drawing made with TURBO (Roussel et al., 1990).

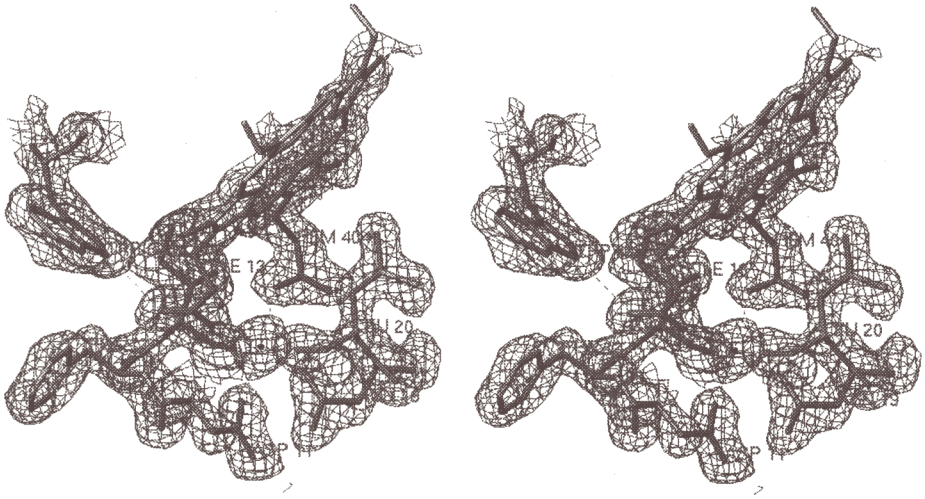

Fig. 10. Stereo view showing the Ca^{2+} ion and the hydrogen bonding pattern involving Phe 12, Trp 68, and heme IV, with superimposed electron density drawn at the 1.0 RMS contour level. Drawing made with TURBO (Roussel et al., 1990).

the Ca^{2+} ion by oxygen atoms from the carboxylate termini of its propionic chains, which adopt in this cytochrome a very different conformation from that found in the other cytochrome c_3 molecules.

Calcium site

The Ca^{2+} ion is coordinated by the six oxygen atoms of the corresponding components of the binding loop and the two propionates of heme IV (see Fig. 3 and Kinemage 1). Within the limits of the resolution, the six-coordinate arrangement is regular octahedral. There is no possibility of a water molecule supplying a seventh coordination position. Table 7 contains a listing of the groups involved, the bond lengths and angles, and the *B*-values of the atoms in the coordination site. The average *B* for the Ca^{2+} and its associated oxygen atoms is 13.7 $Å^2$. This value, which is very close to the average *B*-value for the core of the protein, indicates that the Ca^{2+} is not just an artifact of crystallization and is an integral part of the molecule. Further evidence for this is that the relatively short loop of polypeptide chain and the propionate groups are involved in nearly perfect octahedral coordination to the Ca^{2+}, essentially burying the ion within the molecule.

This is the first instance of finding a bound ion of this kind intimately associated with a cytochrome c_3. Although the reason for this is not obvious, it is clearly a very interesting feature. Not only is the Ca^{2+} ion coordinated by a loop region of the polypeptide chain that is unique to c_3Dg (see Fig. 1), but it is also coordinated by the two propionate groups of heme IV. This coordination places the unique Phe 12 into position to associate with Trp 68, providing a completely different environment for one side of heme II.

The discovery of a Ca^{2+} ion firmly fixed in the c_3Dg molecule was unexpected. The protein was never purposely exposed to calcium during purification and crystallization. In fact, this metal ion was located in the 2.4-Å model (Matias et al., 1994), but was then thought to be magnesium, and elucidation of its chemical nature and coordination geometry was the main objective that led us to carry out a synchrotron data collection experiment. However, the 1.8-Å refinement clearly indicated that this ion could not be magnesium. The initial refinement with a magnesium ion led to a *B*-value for this atom (ca. 5 $Å^2$) significantly lower than the average protein value. Furthermore, the difference electron density map calculated with this model had a very large peak (ca. 13 RMS units, about twice the height of the second highest peak) at the magnesium site. Finally, there

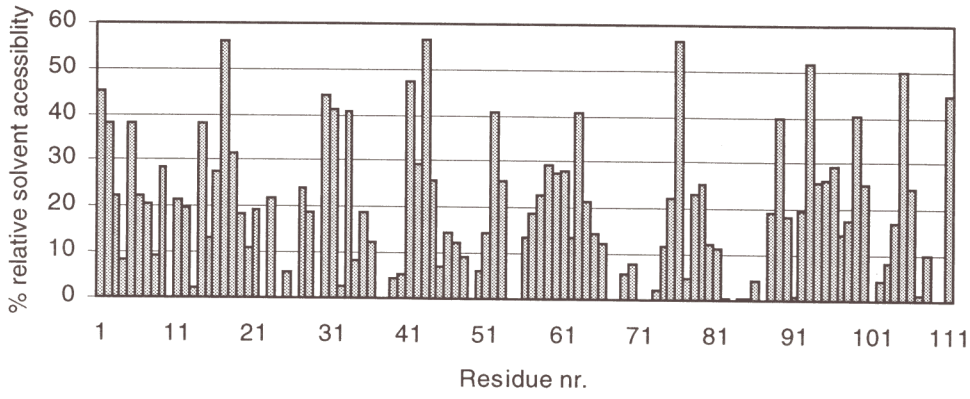

Fig. 11. Relative percent solvent accessibility per residue for c_3Dg.

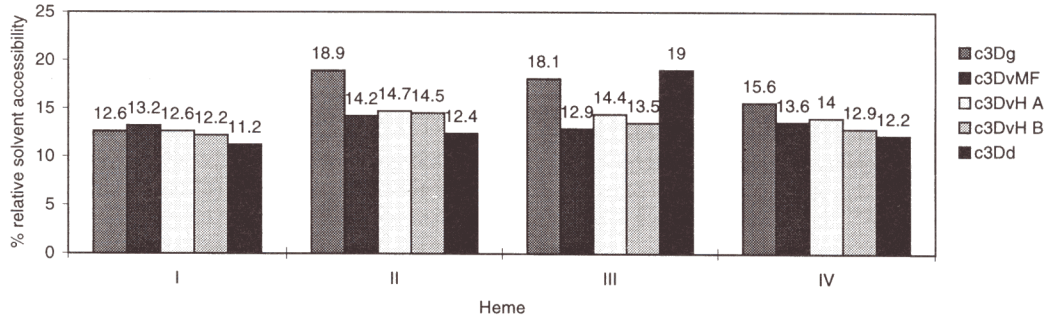

Fig. 12. Relative percent solvent accessibility for the heme groups in c_3Dg, c_3DvH (molecules A and B), c_3DvMF, and c_3Dd.

were no restraints whatsoever applied to the metal–oxygen coordination distances, and the observed distances between the metal and the coordinated oxygen atoms (see Table 7) were found to be significantly longer than the usual values for Mg^{2+}–O distances, and in the expected range for Ca^{2+}–O distances (Fraústo da Silva & Williams, 1991). Despite the fact that Mg^{2+} is more likely to be octahedrally coordinated than Ca^{2+}, the crystallographic evidence strongly suggests that this is indeed a calcium ion.

Although the c_3Dg molecule has the lowest pI of all the c_3 molecules and a somewhat unique segment near the N-terminal portion of the polypeptide chain, there was no reason to expect significant differences in this molecule from other cytochromes of this kind. This cytochrome has about as much homology to the other c_3 sequences as they do to each other, and possesses a rather normal distribution of midpoint redox potentials. In fact, this expected similarity to the other cytochromes contributed to the difficulties in the initial investigation of the crystal structure at 2.4 Å resolution (Kissinger, 1989) when this loop region, containing the Ca^{2+} ion, resisted analysis.

Table 7. *Coordination geometry of the Ca^{2+} ion*

A. Distances (Å) Atom	Distance to Ca^{2+}	B (Å^2)
$O^{\delta 1}$ (Asp 11)	2.30 (3)	13.0
O (Ile 13)	2.22 (3)	13.6
$O^{\delta 1}$ (Asn 19)	2.44 (3)	16.1
O (Leu 20)	2.36 (2)	11.2
O^{1A} (Heme IV)	2.40 (3)	16.6
O^{2D} (Heme IV)	2.25 (2)	9.4
B. Angles around Ca^{2+} ion (°)		
$O^{\delta 1}$ (Asp 11)-Ca^{2+}-O (Ile 13)		88 (1)
$O^{\delta 1}$ (Asp 11)-Ca^{2+}-$O^{\delta 1}$ (Asn 19)		86 (1)
$O^{\delta 1}$ (Asp 11)-Ca^{2+}-O (Leu 20)		89 (1)
$O^{\delta 1}$ (Asp 11)-Ca^{2+}-O^{1A} (Heme IV)		175 (2)
$O^{\delta 1}$ (Asp 11)-Ca^{2+}-O^{2D} (Heme IV)		88 (1)
O (Ile 13)-Ca^{2+}-$O^{\delta 1}$ (Asn 19)		80 (1)
O (Ile 13)-Ca^{2+}-O (Leu 20)		170 (2)
O (Ile 13)-Ca^{2+}-O^{1A} (Heme IV)		91 (1)
O (Ile 13)-Ca^{2+}-O^{2D} (Heme IV)		88 (1)
$O^{\delta 1}$ (Asn 19)-Ca^{2+}-O (Leu 20)		90 (1)
$O^{\delta 1}$ (Asn 19)-Ca^{2+}-O^{1A} (Heme IV)		98 (1)
$O^{\delta 1}$ (Asn 19)-Ca^{2+}-O^{2D} (Heme IV)		167 (2)
O (Leu 20)-Ca^{2+}-O^{1A} (Heme IV)		92 (1)
O (Leu 20)-Ca^{2+}-O^{2D} (Heme IV)		101 (1)
O^{1A} (Heme IV)-Ca^{2+}-O^{2D} (Heme IV)		87 (1)

The Ca^{2+}-binding loop bears some resemblance to the EF-hand (helix-loop-helix) type Ca^{2+}-binding motifs. The first residue that coordinates to the Ca^{2+} ion is an aspartic acid and the sixth residue in the binding loop is a noncoordinating glycine residue, both of which are in similar positions in the EF-hand binding loops. It has been pointed out that a glycine residue is necessary at this position because a side chain would disturb the EF motif (Branden & Tooze, 1991). As can be seen in Figure 3, a large side chain would disrupt the Ca^{2+} coordination in c_3Dg. However, except for these two residues, the binding site in c_3Dg shows some significant differences from the EF motif. The chain folding in c_3Dg does not contain the typical helix-loop-helix observed in the EF motif, nor does the molecule contain more than one binding site, as is found with the typical calcium-binding proteins, such as calmodulin, parvalbumin, and troponin-C, which have been shown to contain two or more EF motifs and possess a regulatory function. Although there is no evidence, it is possible to imagine that the single calcium-binding site in c_3Dg could have some type of regulatory function because it is associated with the two propionate groups of heme IV. In this case, the regulation would more likely affect some aspect of the redox potential of heme IV or possibly contribute to some form of specificity with a redox partner.

Enzymes with calcium involved in their catalytic activity, such as α-amylases (Brayer et al., 1995), tend to have calcium sites that are both solvent and substrate accessible. These calcium sites generally have one or two water molecules coordinated to the calcium ion and are not often found to be coordinated by a set of residues within a relatively short loop (Fraústo da Silva & Williams, 1991; Brayer et al., 1995). Other enzymes, such as horseradish (Haschke et al., 1978), lignin (Poulos et al., 1993) and the di-heme *Paracoccus* cytochrome *c* (Gilmour et al., 1994), peroxidases were found to have bound calcium ions, essential for their activity, maintaining the conformation and integrity of their active site. Recently, the crystal structure of di-heme cytochrome *c* peroxidase from *Pseudomonas aeruginosa* (Fülöp et al., 1995) revealed the presence of a calcium ion in a pentagonal bipyramidal arrangement (four of the seven ligands are water molecules) located at the interface between the two protein domains, each of which contains a covalently attached heme group. The likely function of this calcium ion is to maintain the structure integrity of this enzyme and, due to its special loca-

tion, the authors suggest it may modulate the electron transfer between the two hemes. Clearly, the Ca^{2+} site in c_3Dg does not fit these criteria for being a catalytic calcium.

It is also known (Strynadka & James, 1989) that, in the Ca^{2+}-binding proteins, ions such as Mg^{2+}, Na^+, and K^+ compete, at high concentrations, with Ca^{2+} for the metal-binding site. Several kinetic and equilibrium binding studies in parvalbumins suggest that Ca^{2+} and Mg^{2+} may be involved in the relaxation event following muscle contraction. Also, a report by Chen et al. (1991) has shown that the in vitro coupling of the isolated components, in a reconstituted *D. gigas* electron transfer chain for the reduction of sulfite that included cytochrome c_3, was stimulated by the addition of Ca^{2+} or Mg^{2+} ions. Those authors were able to locate and partially characterize a previously unknown calcium-binding protein in this electron transfer chain.

Considering the competition played between Ca^{2+} and Mg^{2+} in the systems as referred above, and taking into account that the coordination geometry site found in this study is more typical of Mg^{2+} than of Ca^{2+}, it is conceivable that, under appropriate conditions, this molecule might also bind Mg^{2+} with minor structural changes in the local vicinity of the coordination site.

Materials and methods

Diffraction quality crystals of c_3Dg could only be grown by the batch liquid diffusion procedure. This was done using small tubes of approximately 3-mm diameter. Each experiment consisted of gently overlaying a mixture of 10 μL of 0.5 M Tris-maleate, pH 6.5, 1 μL of 1 M sodium azide, 110 μL of 60% PEG 8000, and 150 μL of protein solution, 4–6 mg/mL, onto 50 μL of buffered 60% PEG 8000. To prevent loss of viable material, it was often important to mix into the protein solution a sufficient amount of PEG to bring it near saturation before overlaying the protein solution onto the buffered PEG solution. It is also essential to use freshly isolated and purified protein, otherwise the protein undergoes some form of polymerization and becomes extremely insoluble. The tube containing the liquid diffusion arrangement was sealed with wax. Crystals developed at either room temperature or at 10 °C. The crystallization experiments at room temperature usually had crystals appearing within 2–3 days and continuing to grow for 3–4 weeks. Under these conditions, c_3Dg forms extremely long, red needles. The crystals are orthorhombic, space group $P2_12_12_1$, with unit cell parameters $a = 41.8$ Å, $b = 50.1$ Å, and $c = 51.7$ Å. These cell parameters differ slightly from those reported by Sieker et al. (1986).

The size and quality of crystals were not consistent and only rarely did a crystal grow large enough for data collection. In addition, the crystals had a limited lifetime before deteriorating to a wax-like consistency.

X-ray data collection to 1.8 Å was conducted on beam line X11 at DESY in Hamburg using a wavelength of 0.928 Å and a 180-mm MAR Research image plate system using a crystal with dimensions $0.05 \times 0.05 \times 1.0$ mm^3. The scanned images were processed with the HKL package (Minor, 1993; Otwinowski, 1993). A total of 44,409 measured intensities were merged into 10,315 unique reflections, in the resolution range $1.8 \leq d \leq 36.0$ Å using the CCP4 program package (CCP4, 1994). The data are 98.3% complete overall (96.0% in the higher-resolution shell, $1.8 \leq d \leq 1.83$ Å), with an overall merging R-factor (I) of 0.059 (0.188), and 85.7% (66.9%) of the merged unique intensities greater than $3\sigma(I)$. Table 8 summarizes the statistics for diffraction data.

The structural model was determined by molecular replacement using data to 2.4-Å resolution (Kissinger, 1989) and the coordinates of a previously refined model (Matias et al., 1994). This procedure, rather than a straightforward electron density calculation using the 2.4-Å phases, was deemed necessary in view of the significant difference in cell parameters between the two crystals.

The cross rotation function calculations were conducted using the MERLOT program package (Fitzgerald, 1988). The model was previously rotated by (30°, 45°, 30°) to avoid a near-origin solution, and the model structure factors were then calculated in an orthogonal P1 cell having lengths of about twice the model dimensions in the three spatial directions and using all the protein atoms in the model. The Crowther fast rotation function (Crowther, 1972) was calculated using Bessel functions of order up to 30, a 20-Å Patterson radius cutoff, and all reflections with $F^2_{obs} > 3\sigma(F^2_{obs})$ in resolution range $8 \geq d \geq 4$ Å. The map was calculated in the Eulerian angle range of $0 \leq \alpha \leq 180°$, $0 \leq \beta \leq 90°$, $0 \leq \gamma \leq 360.0°$, with grid steps of 2.5° in α, and 5° in β and γ. A strong peak was observed at $\alpha = 155.0°$, $\beta = 45.0°$, and $\gamma = 145.0°$, with a peak height of 8.5σ (map RMS value), with no noise peaks higher than 60% of the maximum. This orientation was refined to within 1° accuracy by the Lattman rotation function (Lattman & Love, 1972), calculated with the same resolution and intensity cutoffs as above, giving $\alpha = 152.5°$, $\beta = 48.0°$, and $\gamma = 150.0°$.

The Crowther and Blow (1967) $T1$ translation function was calculated using the same resolution and intensity cutoffs as above for each of the three Harker sections in space group $P2_12_12_1$. The translation vector found was (0.075, 0.99, 0.90) in fractional coordinates and the resulting molecular replacement solution was then optimized by R-factor minimization using the same resolution and intensity cutoffs as above to $\alpha = 151.2°$, $\beta = 47.4°$, and $\gamma = 148.2°$; $T_x = 0.075$, $T_y = 0.988$, $T_z = 0.900$, with a 0.1° angular and 0.001 positional accuracy, the crystallographic R-factor being lowered to 34.0%.

The coordinate transformations were then applied to the model. Prior to refinement, the diffraction data were divided into a working set (90%) and a test set (10%) following the procedure by Brünger (1992a). Firstly, 20 cycles of rigid body refinement were performed with X-PLOR (Brünger, 1992b), using

Table 8. *Data collection summary for c_3Dg at 1.8 Å*

X-ray source	DESY-Hamburg station XII
X-ray wavelength	0.928 Å
Resolution range	$1.80 \leq d \leq 36.0$ Å
No. of observations	44,409
No. of independent reflections	10,315
Completeness	98.3% (96.0%)[a]
$\%I > 3\sigma(I)$	85.7% (66.9%)
Merging R-factor (I)[b]	5.9% (18.8%)

[a] Values in parentheses refer to the highest-resolution shell, $1.80 \leq d \leq 1.83$ Å.

[b] $R_{merge} = \sum_{hkl} \sum_j |F_{hkl,j} - \langle F_{hkl} \rangle| / \sum \langle F_{hkl} \rangle$, where j represents replicate measurements of a given reflection (hkl).

all working set reflections in the resolution range $10.0 \geq d \geq 1.8$ Å and $F_{obs} \geq 2\sigma(F_{obs})$. A 3,000-K simulated annealing calculation was then performed using the standard X-PLOR protocol and the *R*-factor lowered to 28.0%, with an *R*-free value of 31.5%. Fourier $2|F_o| - |F_c|$ and $|F_o| - |F_c|$ maps were then computed and extensive model rebuilding was conducted using TOM (Jones, 1978; Cambillau & Horjales, 1987). A large peak near the propionate carboxyl groups of heme IV could be clearly seen, its distances to neighboring protein oxygen atoms being shorter than the usual van der Waals or hydrogen bonding distances, and within the range of coordination distances to calcium ions. This peak had been attributed to a magnesium ion previously (Matias et al., 1994, see discussion). A series of refinement stages using data up to 1.8-Å resolution was performed, in which 50 cycles of positional parameter refinement were followed by 15 cycles of overall *B*-factor refinement, 15 cycles of group *B*-factor refinement, 15 cycles of restrained individual *B*-factor refinement, and finally 50 more cycles of positional refinement. No distance restraints were applied to the Ca^{2+} ion. The atomic *B*-factors were, however, reset to 11.0 $Å^2$ (the approximate value of the overall protein B) each time prior to the overall *B*-factor optimization. After each stage, new $2|F_o| - |F_c|$ and $|F_o| - |F_c|$ maps were computed, and minor model corrections conducted. Also, these maps were used to locate a number of water molecules. The final XPLOR *R*-factor was 19.3% and the *R*-free was 24.1%. The final refinement cycles were performed with SHELXL-93 (Sheldrick & Schneider, 1996) using a restrained conjugated gradient weighted least-squares procedure on F^2. New $2|F_o| - |F_c|$ and $|F_o| - |F_c|$ maps were used to perform minor model corrections as well as to locate additional water molecules. The criteria for including a water molecule were that the corresponding peak should be visible in both the $2|F_o| - |F_c|$ and $|F_o| - |F_c|$ Fourier maps, and make reasonable hydrogen bonds to neighboring donor or acceptor groups. Solvent molecules for which the refined *B*-value exceeded 50.0 were regarded as partially occupied water sites, with an occupation factor arbitrarily set at 0.5. A final refinement was performed using overlapping block-matrix weighted least squares, in order to obtain estimated standard deviations for the atomic parameters (positional and isotropic thermal motion parameters). The final *R*-factor obtained was 14.9%, with an *R*-free of 21.9% based on a random sample of 10% of the measured reflections with $F \geq \sigma(F)$. Table 9 lists a summary of the final refinement statistics. The final atomic coordinates of the refined structural model have been deposited in the Protein Data Bank (Bernstein et al., 1977; Abola et al., 1987), with entry code 1WAD and accession date January 8, 1997.

Table 9. *Final refinement statistics for the structure of c_3 D. gigas*

Resolution limits (Å)	36.0–1.8
No. reflections used	9,125 with $F_o \geq \sigma(F_o)$
No. of restraints	10,863
No. of protein atoms	1,008
No. of solvent molecules	58 (Full occupancy)
	44 (Partial occupancy)
Final *R*-factor (%)[a]	14.9
Final *R*-free (%)	21.9
No. of disagreeable restraints	3

[a] $R\text{-factor} = 100 * \sum|F_o - F_c| / \sum|F_o|$.

Acknowledgments

We thank Dr. Charles Kissinger for his earlier involvement in the structural work at 2.4 Å, Prof. Jean LeGall and Dr. Ming-Yih Liu for supplying us with protein samples, Ms. Isabel Pacheco for purifying the protein, and Profs. António V. Xavier and Jean LeGall for many helpful discussions and suggestions during the course of this work. Financial support from the European Commission (Network CHRX-CT93-0143 and BIO2-CT94-2052, HCMP Large Installation Project CHGE-CT93-0040 and research project PRAXIS/2/2.1/QUI/17/94) and JNICT (PBICT/BIO/1277/92, fellowship BD/2155/92-IE to J.M. and PRAXIS grant GGP XXI/BIC/911/95 to R.C.) is also gratefully acknowledged.

References

Abola EE, Bernstein FC, Bryant SH, Koetzle TF, Weng J. 1987. Protein Data Bank. In: Allen FH, Bergeroff G, Sievers R, eds. *Crystallographic databases—Information content, software systems, scientific applications*. Bonn/Cambridge/Chester: Data Commission of the International Union of Crystallography. pp 107–132.

Bernstein FC, Koetzle TF, Williams GJB, Meyer EF Jr, Brice MD, Rodgers JR, Kennard O, Shimanouchi T, Tasumi M. 1977. The Protein Data Bank: A computer-based archival file for macromolecular structures. *J Mol Biol 112*:535–542.

Branden C, Tooze J. 1991. *Introduction to protein structure*. New York/London: Garland Publishing.

Brayer G, Luo Y, Withers SG. 1995. The structure of human pancreatic α-amylase at 1.8 Å resolution and comparisons with related enzymes. *Protein Sci 4*:1730–1742.

Brünger AT. 1992a. Free *R* value: A novel statistical quantity for assessing the accuracy of crystal structures. *Nature 355*:472–474.

Brünger AT. 1992b. *XPLOR: A system for X-ray crystallography and NMR*. New Haven, Connecticut: Yale University Press.

Cambillau C, Horjales E. 1987. TOM: A FRODO subpackage for protein–ligand fitting with interactive energy minimization. *J Mol Graphics 5*: 175–177.

CCP4. 1994. Collaborative Computational Project Number 4. The CCP4 suite: Programs for protein crystallography. *Acta Crystallogr D 50*: 760–763.

Chen L, Liu MY, LeGall J. 1991. Calcium is required for the reduction of sulfite from hydrogen in a reconstituted electron transfer chain from the sulfate reducing bacterium *Desulfovibrio gigas*. *Biochem Biophys Res Commun 180*:238–242

Coelho AV, Matias P, Frazão C, Carrondo MA. 1995. Crystal structure of c_3 cytochrome from *D. baculatus* ATCC 9974 at 1.8 Å resolution. Como, Italy: Fourth European Workshop on Crystallography of Biological Macromolecules.

Crowther RA. 1972. The fast rotation function. In: Rossmann MG, ed. *The molecular replacement method*. New York: Gordon and Breach. pp 173–178.

Crowther RA, Blow DM. 1967. A method of positioning a known molecule in an unknown crystal structure. *Acta Crystallogr 23*:544-548.

Czjzek M, Payan F, Guerlesquin F, Bruschi M, Haser R. 1994. Crystal structure of cytochrome c_3 from *Desulfovibrio desulfuricans* Norway at 1.7 Å resolution. *J Mol Biol 243*:653–667.

Fitzgerald PM. 1988. MERLOT, an integrated package of computer programs for determination of crystal structures by molecular replacement. *J Appl Crystallogr 21*:273–278.

Fraústo da Silva JJR, Williams RJP. 1991. *The biological chemistry of the elements: The inorganic chemistry of life*. Oxford, UK: Clarendon Press.

Fülöp V, Ridout CJ, Greenwood C, Hajdu J. 1995. Crystal structure of the di-haem cytochrome *c* peroxidase from *Pseudomonas aeruginosa*. *Structure 3*:1225–1233.

Gilmour R, Goodhew CF, Pettigrew GW, Prazeres S, Moura JJG, Moura I. 1994. The kinetics of the oxidation of cytochrome *c* by *Paracoccus* cytochrome *c* peroxidase. *Biochem J 300*:907–914.

Haschke RH, Friedhoff JM. 1978. Calcium related properties of horseradish peroxidase. *Biochem Biophys Res Commun 80*:1039–1042.

Higuchi Y, Akutsu H, Yasuoka N. 1994. A detailed comparison of the refined structures of cytochrome c_3 molecules from two strains in *Desul-*

fovibrio vulgaris: The relationship between the heme structures and their redox properties. *Biochimie 76*:537–545.
Higuchi Y, Kusunoki M, Matsuura Y, Yasuoka N, Kakudo M. 1984. Refined structure of cytochrome c_3 at 1.8 Å resolution. *J Mol Biol 172*:109–139.
Jones TA. 1978. A graphics model building and refinement system for macromolecules. *J Appl Crystallogr 11*:268–272.
Kissinger C. 1989. [thesis]. Seattle, Washington: Washington University.
Laskowski RA, MacArthur MW, Moss DS, Thornton JM. 1993. PROCHECK: A program to check the stereochemical quality of protein structures. *J Appl Crystallogr 26*:283–291.
Lattman EE, Love WE. 1972. A rotational search procedure for detecting a known molecule in a crystal. *Acta Crystallogr B 26*:1854–1857.
Lee B, Richards FM. 1971. The interpretation of protein structures: Estimation of static accessibility. *J Mol Biol 55*:379–400.
LeGall J, Hazza G, Dragoni N. 1963. Le cytochrome c_3 de *Desulfovibrio gigas*. *Biochim Biophys Acta 56*:385–387.
Matias PM, Frazão C, Morais J, Coll M, Carrondo MA. 1993. Structure analysis of cytochrome c_3 from *Desulfovibrio vulgaris* Hildenborough at 1.9 Å resolution. *J Mol Biol 234*:680–699.
Matias PM, Kissinger C, Carrondo MA, Sieker L. 1994. Structure analysis of cytochrome c_3 from *Desulfovibrio gigas* at 2.4 Å resolution. Atlanta, Georgia: 1994 ACA Meeting.
Minor W. 1993. *XDISPLAYF program*. West Lafayette, Indiana: Purdue University.
Morais J, Palma PN, Frazão C, Caldeira J, LeGall J, Moura I, Moura JJG, Carrondo MA. 1995. Structure of the tetraheme cytochrome from *Desulfovibrio desulfuricans* ATCC 27774: X-ray diffraction and electron paramagnetic resonance studies. *Biochemistry 34*:12830–12841.
Morimoto Y, Tani T, Okumura H, Higuchi Y, Yasuoka N. 1991. Effects of amino acid substitution on the three-dimensional structure: An X-ray analysis of cytochrome c_3 from *Desulfovibrio vulgaris* Hildenborough at 2 Å resolution. *J Biochem 110*:532–540.
Otwinowski Z. 1993. Oscillation data reduction program. In: Sawyer L, Isaacs N, Bailey S, eds. *Proceedings of the CCP4 Study Weekend: "Data Collection and Processing"*. Warrington, UK: SERC Daresbury Laboratory. pp 56–62.
Piçarra-Pereira MA, Turner DL, LeGall J, Xavier AV. 1993. Structural studies on *Desulfovibrio gigas* cytochrome c_3 by two-dimensional ^{1}H-nuclear-magnetic-resonance spectroscopy. *Biochem J 294*:909–915.
Poulos TL, Edwards SL, Wariishi H, Gold MH. 1993. Crystallographic refinement of lignin peroxidase at 2 Å. *J Biol Chem 268*:4429–4440.
Ramachandran GN, Sasisekharan V. 1968. Conformation of polypeptides and proteins. *Adv Prot Chem 23*:283–437.
Read RJ. 1986. Improved fourier coefficients for maps using phases from partial structures with errors. *Acta Crystallogr A 42*:140–149.
Roussel A, Fontecilla-Camps JC, Cambillau C. 1990. TURBO-FRODO: A new program for protein crystallography and modelling. Bordeaux, France: XV IUCr Congress.
Santos H, Moura JJG, Moura I, LeGall J, Xavier AV. 1984. NMR studies of electron transfer mechanisms in a protein with interacting redox centers: *Desulfovibrio gigas* cytochrome c_3. *Eur J Biochem 141*:283–296.
Sieker LC, Jensen LH, LeGall J. 1986. Preliminary X-ray studies of the tetraheme cytochrome *c*3 and the octa-heme cytochrome c_3 from *Desulfovibrio gigas*. *FEBS Lett 209*:261–264.
Sheldrick GM, Schneider TM. 1996. SHELXL: High-resolution refinement. *Methods Enzymol*. Forthcoming.
Strynadka NCJ, James MNG. 1989. Crystal structures of the helix-loop-helix calcium-binding proteins. *Annu Rev Biochem 5*:951–998.